AIMS Biophysics, 3(3): 340-357.
DOI: 10.3934/biophy.2016.3.340
Received: 06 June 2016
Accepted: 20 July 2016
Published: 22 July 2016

http://www.aimspress.com/journal/biophysics

Research article

Viscoelastic capillary flow: the case of whole blood

David Gosselin [1,2,3,4,5,*], Maxime Huet [1,2], Myriam Cubizolles [1,2], David Rabaud [1,2], Naceur Belgacem [3,4,5], Didier Chaussy [3,4,5], and Jean Berthier [1,2]

[1] Univ. Grenoble Alpes, F-38000 Grenoble, France
[2] CEA LETI MINATEC Campus, F-38054 Grenoble France.
[3] University Grenoble Alpes, LGP2, F-38000 Grenoble, France
[4] CNRS, LGP2, F-38000 Grenoble, France
[5] Agefpi, LGP2, F-38000 Grenoble, France

* **Correspondence:** Email: david.gosselin@cea.fr.

Abstract: The dynamics of spontaneous capillary flow of Newtonian fluids is well-known and can be predicted by the Lucas-Washburn-Rideal (LWR) law. However a wide variety of viscoelastic fluids such as alginate, xanthan and blood, does not exhibit the same Newtonian behavior.

In this work we consider the Herschel-Bulkley (HB) rheological model and Navier-Stokes equation to derive a generic expression that predicts the capillary flow of non-Newtonian fluids. The Herschel-Bulkley rheological model encompasses a wide variety of fluids, including the Power-law fluids (also called Ostwald fluids), the Bingham fluids and the Newtonian fluids. It will be shown that the proposed equation reduces to the Lucas-Washburn-Rideal law for Newtonian fluids and to the Weissenberg-Rabinowitsch-Mooney (WRM) law for power-law fluids. Although HB model cannot reduce to Casson's law, which is often used to model whole blood rheology, HB model can fit the whole blood rheology with the same accuracy.

Our generalized expression for the capillary flow of non-Newtonian fluid was used to accurately fit capillary flow of whole blood. The capillary filling of a cylindrical microchannel by whole blood was monitored. The blood first exhibited a Newtonian behavior, then after 7 cm low shear stress and rouleaux formation made LWR fails to fit the data: the blood could not be considered as Newtonian anymore. This non-Newtonian behavior was successfully fit by the proposed equation.

Keywords spontaneous capillary flow; whole blood; non-Newtonian fluid; RBCs rouleaux; Herschel-Bulkley fluids; viscoelastic fluids; yield stress

1. Introduction

Capillary flow of Newtonian fluids is abundantly reported in the literature. First in the case of cylindrical duct with the Lucas-Washburn-Rideal law [1–4] and then extended to a large number of other channel geometries [5,6]. Recent studies have investigated the capillary flow of Newtonian liquids within non-uniform channels [7–10].

Capillary flows are of interest for point-of-care (POC) and home-care systems since they must be low cost, energetically autonomous, portable, and user-friendly. Blood from a finger prick is a very common biological sample for POC and many of them rely on capillarity to move the blood through the different parts of the system [11–13]. However the capillary flow of whole blood is conditioned by its complicated rheology linked to the multiplicity and variability of its components, such as plasma, red blood cells, white blood cells, platelets, etc.

Whole blood shows different rheological regimes according to the shear rate it is exposed to [14–17]. On one hand, for high shear rates ($\dot{\gamma} > 100$ s^{-1}), blood exhibits a Newtonian behavior and its viscosity μ_0 is constant and given by

$$\mu_0 = \frac{\tau}{\dot{\gamma}} \tag{1}$$

where $\dot{\gamma}$ is the shear rate and τ the shear stress. On the other hand, for low shear rates ($\dot{\gamma} < 30$ s^{-1}) whole blood exhibits a non-Newtonian rheology, which is often modeled by Casson's law [14–16]. Casson's law links the shear stress τ to the shear rate $\dot{\gamma}$ by the expression

$$\sqrt{\tau} = \sqrt{\tau_0} + \sqrt{\mu_0 \dot{\gamma}} \tag{2}$$

where τ_0 is the yield stress. Relation (2) indicates that if the shear stress τ is not larger than τ_0, there is no shear rate ($\dot{\gamma} = 0$). In other words, when the shear stress is not high enough, the fluid behaves as a solid, with an infinite viscosity. This can be explained by the fact that, contrary to high shear rate which would disperse the red blood cells, the red blood cells tend to aggregate and form rouleaux at small shear rates. This aggregation gives to the blood its non-Newtonian behavior [17–19].

Besides, in the case of a medium flow velocity and/or diluted blood, cells tends to migrate away from the walls forming a cell-free layer. This phenomenon is sometimes called the Vand effect, or the Farhaeus-Lindqvist effect [20,21]. Note that this effect is not very apparent in the case of whole blood spontaneous capillary flow because the velocities are relatively small. In accordance, it will not be taken into account in this study.

In this work, the Herschel-Bulkley (HB) rheological model [22] is used to derive a general equation for the dynamics of capillary flow for non-Newtonian fluids. This model encompasses a

wide variety of fluids, including the Power-law fluids (also called Ostwald fluids), the Bingham fluids and the Newtonian fluids. The constitutive equations of this model are given by:

$$\begin{aligned} &\dot{\gamma} = 0 \quad if \ \ \tau < \tau_0 \\ &\tau = \left(\frac{\tau_0}{|\dot{\gamma}|} + K|\dot{\gamma}|^{n-1} \right) \dot{\gamma} \quad if \ \ \tau > \tau_0 \end{aligned} \tag{3}$$

where K and n are two rheological parameters depending on the fluid. Just like the Casson's law, the HB model allows the yield stress to be taken into account but it has an additional degree of freedom which is the n parameter. Note that if $\tau_0 = 0$ this law reduces to the well-known power-law. The fluid is then said shear-thinning if n < 1 and shear-thickening if n > 1. On the other hand if n = 1 (and $\tau_0 \neq 0$), a Herschel-Bulkley fluid is called a Bingham fluid [23,24]. Finally if n = 1 and $\tau_0 = 0$, equation (3) reduces to the classical Newtonian relationship between the shear rate, the shear stress and the viscosity (Eq 1). Although the HB model cannot be reduced to the Casson's law—which is usually used for whole blood, it also describes accurately the non-Newtonian rheological behavior of whole blood, as we shall see later. Using the HB model, it will be shown that the proposed generalized equation accurately fit experimental data of whole blood flowing through cylindrical capillaries.

Recently studies were conducted on capillary flow of power-law fluids [25,26]. Although the authors used blood for some of their experiments, their theoretical model could not take the effect of the yield stress into account. The present work is based on the HB law, and provides a very general model for the flow of non-Newtonian fluids with or without yield stress. It will also be demonstrated that the proposed equation consistently reduces to previously described laws for Newtonian fluids—the LWR law [1–4] and Power-law fluids—the Weissenberg-Rabinowitsch-Mooney (WRM) law [23,27,28].

2. Materials and Methods

2.1. Monitoring of the capillary filling

Blood flow experiments were performed in glass tubular micro-channels of inner radius 50μm (CM scientific, VitroCom). More precisely the micro-channels are made with the Schott's Duran Borosilicate 3.3. The radius of the tubes has been chosen to be consistent with the one of typical microchannels used for in-vitro point-of-care devices. The commercialized micro-channels are 60 cm long, but for convenience for the experiments, were cut to the length of 20 cm.

The micro-channel is glued (Scotch 3M) in an outlet channel of a reservoir (Figure 1). The outlet is 1 mm wide and 10 mm long and the reservoir is 10 mm in diameter; both are 1 mm deep. They are milled from PMMA substrate using a CNC milling machine (Charly4U, charlyrobot). This reservoir offers a volume of 80 μL which is large compared to the volume of the cylindrical channels (1.6 μL). The large dimensions of the reservoir ensure that the curvature of the meniscus is negligible and that the air-liquid interface remains flat during the filling—so that the Laplace pressure of the reservoir is null or negligible. The meniscus height is low enough to neglect the added hydrostatic

pressure. Thus the reservoir provides a liquid supply at nearly atmospheric pressure during the whole experiment.

The reservoir was taped on a plastic holder, itself attached to a millimeter paper, to avoid any displacement of the set up during the experiment.

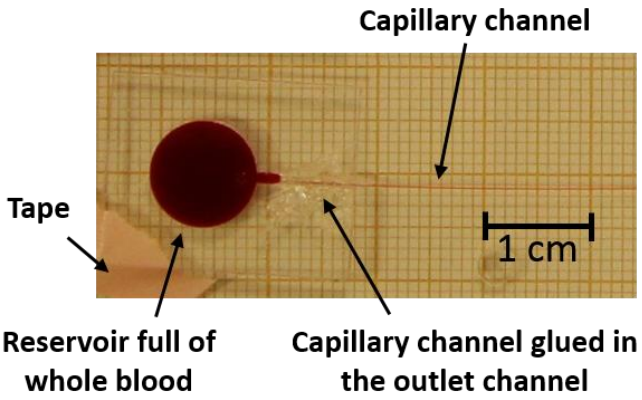

Figure 1. Set-up of the experiment. The microchannel is connected to the reservoir and fixed in the reservoir outlet channel using glue.

The filling distance was monitored during the capillary filling with a Canon EOS 600D fixed on a tripod. A snapshot was taken every 2 seconds using a timer remote controller during the whole experiment. Because all the set up was fixed, the monitoring of the filling distance is easily done by recording the corresponding distance of the front interface (Figure 2) on the millimeter paper. By this method, a precision of 0.3 mm can be achieved.

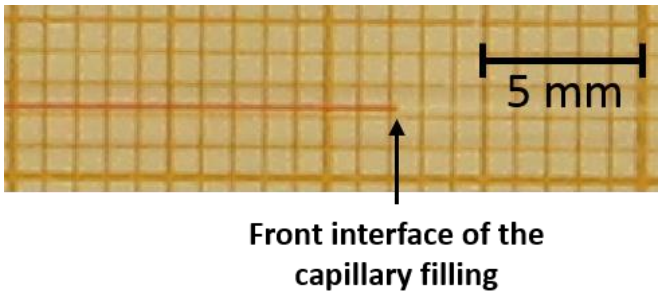

Figure 2. Microchannel and position of the front interface. The filling distance is obtained by looking at the corresponding position on the millimeter paper.

2.2. Blood sample

A blood sample from a healthy donor (Etablissement Français du Sang (EFS), Grenoble, FRANCE) collected in EDTA (Ethylenediaminetetraacetic acid) vacutainer tubes (Becton Dickinson) was used for the experiments. According to the ethical and legal standards of our blood supplier

(EFS), informed consent was given by blood donor. The blood tube was delivered 3 days after withdrawal and was refrigerated at 4 ℃ for storage. The experiments were performed the day of delivery.

For this study we will assume the value of 60mN/m for the surface tension of whole blood, which is a typical value for healthy people at the temperature of which the experiments are conducted, i.e. 21 ℃ [29].

2.3. The Herschel-Bulkley model for whole blood.

The general HB law is used to model the non-Newtonian behavior in the present work. To determine the rheological constants (τ_0, K and n) of whole blood needed for this work, data collected from three previous studies in [30] are used. In figure 3, the circles depict these data whereas the red solid line represents the Herschel-Bulkley model obtained by fitting the data with the cftool toolbox of MATLAB (MathWorks). This fit gives a R^2 coefficient of 0.98 and the rheological parameters of Table 1.

Table 1. Blood rheological parameters obtained from the Herschel-Bulkley fit of data extracted from [30].

Blood rheological parameters
$\tau_0 = 0.01397\ Pa$
$K = 0.0106\ \text{Pa}.s^n$
$n = 0.788$

The blue dashed curve of Figure 3 depicts a fit using the Casson's law—R^2 coefficient of 0.98. This figure shows that, just like the Casson's law, the HB law is well suited for describing the non-Newtonian rheological behavior of whole blood. Thus the choice of the HB model over the usual Casson's law is not an issue to model the capillary flow of whole blood.

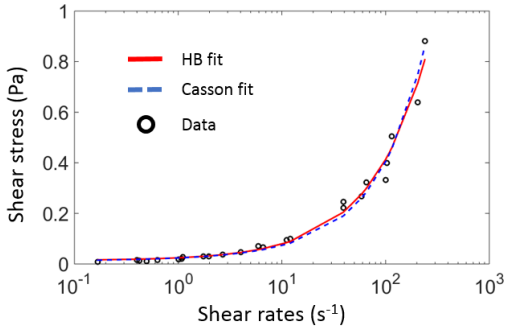

Figure 3. Circles: Data extracted from [30]. Red solid line: Fit with the Herschel-Bulkley model using the rheological parameters given in Eq (4). Blue dashed line: Fit with the Casson's law.

2.4. Fit of the non-Newtonian flow.

In the Results and Discussions section, a differential equation for dynamics of non-Newtonian capillary flow is derived from the Navier-Stokes equation. Although most of the coefficients are known—see previous subsections of Materials and Methods for the rheological coefficients, channel dimensions, and blood surface tension—one coefficient of the equation remains unknown: the contact angle θ between blood and the borosilicate tube. In order to determine θ, the mean square error between experimental results and the solutions of our model (see equation (6)) computed with θ varying between 50° and 70° is calculated. It is done with the MATLAB software using the ode45 function. The contact angle is then the value which gives the smallest mean square error. For this numerical method, only the data points falling in the non-Newtonian regime have to be taken into account. By looking at the plot of the filling distance versus the square root of time, one can see that the data points start to deviate from the linear relationship characterizing the Newtonian regime around 7 cm from the inlet. Thus only the data points at a distance farther than 7 cm from the inlet are used for the non-Newtonian fitting.

2.5. Fit of the Newtonian flow.

The fitting of the Newtonian part of the flow is done using Microsoft Excel software. The Newtonian behavior is a proper description of the blood rheology at the beginning of the capillary flow when the velocity of the flow is high and the shear rate disperses the red blood cells. Although the data points seem deviate from the Newtonian regime only after 7 cm, a transition regime can be expected during the few preceding centimeters. Thus the Newtonian fitting will only use data points until 5 cm. In addition, at the very beginning of a capillary flow inertia and dynamic contact angle influence the dynamics [31,32]. Previous studies have established that after a few millimeters the dynamic contact angle is nearly the same as the static contact angle [33]. Thus to avoid these effects the Newtonian fit starts only after the first two centimeters. Note that the contact angle for the Newtonian regime is the same as the one previously determined with the fitting of the viscoelastic regime.

3. Results and Discussions

3.1. The Newtonian—non Newtonian transition

By plotting the filling distance against the square root of time, one can observe two different behaviors (Figure 4). First the filling distance evolves linearly with the square root of time as expected for a Newtonian fluid. But after a few centimeters (around 7 cm) this relation is no longer true.

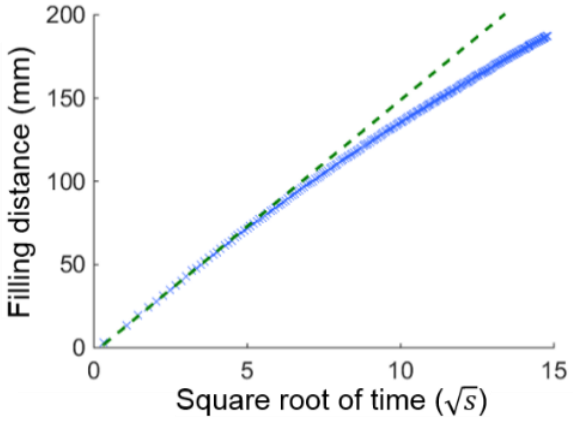

Figure 4. In the first centimeters the filling distance of whole blood inside a borosilicate cylindrical microchannel evolves linearly with the square root of time. Afterwards the data points (blue crosses) depart from the Newtonian linear fit (green dashed-line).

This transition of behavior is consistent with the expected rheological behaviors of undiluted whole blood. Indeed at the beginning of the capillary flow there is very little friction with the walls and the velocity of the flow is relatively high (a few mm/s). This results in a high shear rate which disperses the RBCs and the blood exhibits a Newtonian behavior [17–19]. As the capillary flow advances in the capillary channel, drag increases and velocity decreases. Along with the decrease in velocity, the shear rate also decreases and RBCs start aggregating together [17–19], leading to the non-Newtonian collective behavior of the fluid.

To quantify this decrease, the shear rate profile has been calculated along the radius of the tube after either 1 cm or 7 cm of capillary flow. Since in this first part of the flow the whole blood has a Newtonian behavior, the shear rate is linear with the radius and can be easily obtained from the Newtonian parabolic Poiseuille profile. Doing such a calculation, it is shown that after 7 centimeters of capillary flow the shear rate has been divided by seven (at the wall, it decreases from 930 s^{-1} to 130 s^{-1}). This large decrease of the shear rate, allowing the formation of rouleaux, can thus explain the Newtonian – non Newtonian transition.

In the following subsections, fits between theory and experiments will be presented for the two rheological behaviors of whole blood. The Lucas-Washburn-Rideal law is well-established for the Newtonian capillary filling of a tube. However two unknowns remain for this part of the flow: the Newtonian viscosity of the blood sample and the contact angle of whole blood with the borosilicate walls. On the contrary, because the Herschel-Bulkley parameters were determined in the Materials and Method section, only the contact angle remains as an unknown for the non-Newtonian part of the flow. That is why the dynamics of the non-Newtonian regime of the capillary filling is first investigated, allowing a consistent determination of the contact angle by a fit with the experiments. Afterwards using this value of contact angle, the Newtonian regime of the capillary filling is analyzed.

3.2. The dynamics of a Herschel-Bulkley capillary filling

In the general case (arbitrary cross-section, open or closed) of a uniform channel, the dynamic of the capillary flow of a Herschel-Bulkley fluid is given by the following differential equation directly obtained via the Navier-Stokes equations (see calculation in Appendix A):

$$\frac{d^2x}{dt^2} + \frac{p_w}{\rho\, A}\frac{K}{\overline{\lambda^n}}\left(\frac{\partial x}{\partial t}\right)^n - \frac{\sigma\, p_w \cos\theta^*}{\rho\, A\, x(t)} = -\frac{p_w}{\rho\, A}\tau_0 \tag{4}$$

where x is the filling distance, t is the time, p_w is the wetting perimeter, A is the cross section area, $\overline{\lambda^n}$ is the average generalized friction length (defined in Appendix A (A.10) as an extension to the friction length introduced in [6]), σ is the surface tension, θ* is the generalized Cassie angle and ρ the fluid density. More details on these different notations can be found in the Appendix A.

The complexity of the problem is hidden in the average generalized friction length $\overline{\lambda^n}$. Its expression, in the particular case of a cylindrical duct, is calculated in appendix B. Using expression B.22 of Appendix B and the fact that the channel is made of a single material (θ* = θ), Eq (4) becomes:

$$\frac{d^2x}{dt^2} + \frac{2}{\rho\, R}K\left(\frac{n+1}{n}\frac{1}{R\,\alpha}\right)^n(1-c)\left(\frac{\partial x}{\partial t}\right)^n - \frac{2\gamma\cos\theta}{\rho\, R\, x(t)} = -\frac{2}{\rho\, R}\tau_0. \tag{5}$$

where R is the radius of the channel, α and c are two dimensionless coefficients which expressions are given in Appendix B.

Because in micro-channels the Reynolds and Weber numbers are small, and even more so in the viscoelastic regime corresponding to small shears, the inertial term can be neglected in a similar manner as for the LWR law, and (5) simplifies to

$$x\left(\frac{dx}{dt}\right)^n = \frac{1}{(1-c)}\frac{1}{K\left(\frac{n+1}{n\,R\,\alpha}\right)^n}(\gamma\cos\theta - x\,\tau_0) \tag{6}$$

Note that in the case of a Newtonian fluid, $n = 1$, $\tau_0 = 0$, $\alpha = 1/2$, $K = \mu$, and expression (6) reduces to the Lucas-Washburn-Rideal law.

Unfortunately direct integration of equation (6) is not possible for Herschel-Bulkley fluids and a closed-form solution does not exists. Thus numerical integration is required to obtain the solution for x(t).

However, note that in the simplified case of a power-law fluid, (6) simplifies to

$$x^{\frac{1}{n}}\frac{dx}{dt} = \left[\frac{1}{K\left(\frac{n+1}{n\,R\,\alpha}\right)^n}\gamma\cos\theta\right]^{\frac{1}{n}}. \tag{7}$$

which can be integrated into the following closed-form

$$x = \left[\frac{n+1}{3n+1}\frac{R^n}{K}\gamma\cos\theta\right]^{\frac{1}{n+1}} t^{\frac{n}{n+1}}. \tag{8}$$

which is the Weissenberg-Rabinowitsch-Mooney (WRM) law. Equation (6) appears to be the generalization of the WRM law for HB fluids.

3.3. Capillary flow of whole blood

3.3.1. The non-Newtonian viscoelastic regime

Table 2 summarizes the contact angle values and the associated mean square errors obtained by the fitting method explained in the experimental section using the numerical integration of (6). Three experiments with three different channels (of same section) have been performed.

Table 2. Values of contact angle and Mean Square Error (MSE) obtained by the fitting of non-Newtonian part of the flow.

	Channel 1	Channel 2	Channel 3
Contact angle	55.7°	56.2°	54.8°
MSE ($\times 10^{-5}$)	3.1	0.56	2.6

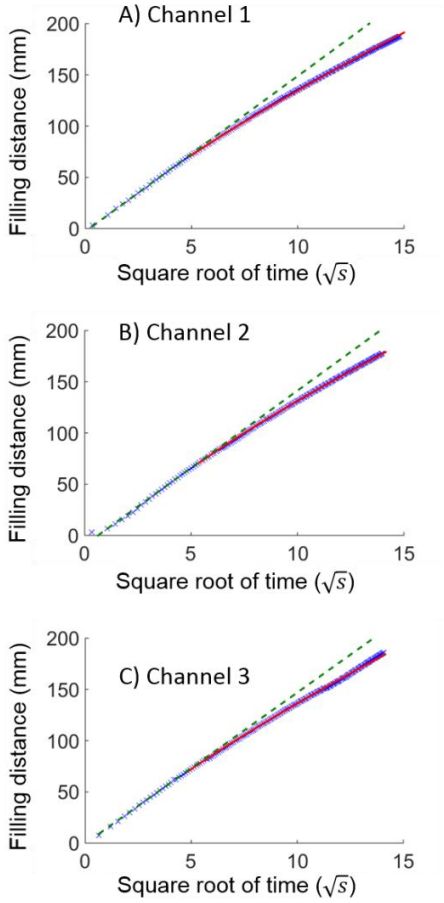

Figure 5. Comparison between the non-Newtonian model of the capillary flow of whole blood (red solid line) and the experimental data points (blue crosses). The green dashed-line shows the Newtonian fit of the first part of the capillary flow.

The different values of contact angle obtained for the three experiments are very close to each other. Besides the very low MSE values show that our modeling of the non-Newtonian part of the flow is valid. Figure 5 shows that the non-Newtonian red curves plotted using θ from table 2 are in good agreements with the experimental data points (blue crosses). On the one hand this demonstrates that the equation (6) is a suitable model for the non-Newtonian capillary flow. On the other hand it confirms the consistency of the Herschel-Bulkley model for whole blood.

3.3.2. The Newtonian regime

The law for the capillary filling of cylindrical duct by a Newtonian fluid is known for decades and is given by [1–4]:

$$x = \sqrt{\frac{\gamma}{\mu}\frac{R}{2}\cos\theta}\sqrt{t} \tag{9}$$

The slope β of the linear function $x \propto \sqrt{t}$ determines the viscosity of dispersed whole blood. Using the different experiments, the viscosity is determined by the formula

$$\mu = \frac{R * \gamma * \cos\theta}{2 * \beta^2} \tag{10}$$

Table 3. Values of viscosity deduced from the linear fit of the Newtonian part of the flows.

	Channel 1	Channel 2	Channel 3
Viscosity (mPa.s)	3.67	3.67	3.87

Table 3 summarizes the value of viscosity obtained with each of the three Newtonian fits. In ref [30] Cherry and Eaton use a value of 0.004 kg/m/s (or 4mPa.s) for the blood viscosity at high shear rate (i. e. in the Newtonian regime). The values obtained in our study are thus in accordance with such classical blood viscosity values. Finding consistent values of high shear rate viscosities for the whole blood confirms again the validity of the generalized equation (6) which has been used to determine the contact angle of the whole blood with the borosilicate tubes.

4. Conclusion and Perspectives

Rheology of whole blood is complicated due to its composition. It is known that, according to the shear rate, its behavior can be depicted by 2 regimes: a Newtonian regime for high shear rates, and a non-Newtonian regime for small shear rates. In this work, we have investigated the capillary filling of whole blood within a 50μm-radius cylindrical duct made of borosilicate. By plotting the filling distance against time we were able to distinguish the two characteristic rheological behaviors of the blood.

On the one hand, the filling distance first follows the Newtonian Lucas-Washburn-Rideal law, i.e. is linear with the square root of time. On the other hand, after a few centimeters (around 7 cm for our 50 μm radius tubes) it departs from the LWR law, meaning that it undergoes a transition towards its non-Newtonian behavior. In this paper a general differential equation for the dynamics of capillary flow of Herschel-Bulkley fluids is derived from the Navier-Stokes equations. The numerical solutions obtained from this equation are in close agreement with the different experiments conducted. This approach demonstrates the validity of the generalized equation for the dynamics of non-Newtonian capillary flows and confirms the consistency of the Herschel-Bulkley model for the whole blood rheology.

Although only whole blood was used for this study, the model proposed in this work profits from the generality of the Herschel-Bulkley law and can be used for the capillary flow of viscoelastic fluids. Capillary flows of fluids such as alginates and xanthan used in biology and biotechnology are now predictable.

Conflict of Interest

The authors declare no conflict of interests.

References

1. Lucas R (1918) Ueber das Zeitgesetz des kapillaren Aufstiegs von Flussigkeiten. *Kolloid-Z.* 23: 15–22.
2. Washburn EW (1921) The dynamics of capillary flow. *Phys Rev* 17: 273–283.
3. Rideal EK (1922) On the flow of liquids under capillary pressure. *Philos Mag Ser* 6: 1152–1159.
4. Bosanquet C (1923) On the flow of liquids into capillary tubes. *Philos Mag Ser* 6: 525–553.
5. Ouali FF, McHale G, Javed H, et al. (2013) Wetting considerations in capillary rise and imbibition in closed square tubes and open rectangular cross-section channels. *Microfluid Nanofluid* 15: 309–326.
6. Berthier J, Gosselin D, Berthier E (2015) A generalization of the Lucas-Washburn-Rideal law to composite microchannels of arbitrary cross section. *Microfluid Nanofluid* 19: 497–507.
7. Erickson D, Li D, Park CB (2002) Numerical simulations of capillary-driven flows in non-uniform cross-sectional capillaries. *J Colloid Interf Sci* 250: 422–430.
8. Elizalde E, Urtega R, Koropecki RR, et al. (2014) Inverse Problem of Capillary Filling. *PRL* 112, 134502.
9. Berthier J, Gosselin D, Pham A, et al. (2016) Spontaneous capillary flows in piecewise varying cross section microchannels. *Sens Actuators B* 223: 868–877.
10. Berthier J, Gosselin D, Pham A, et al. (2016) Capillary Flow Resistors: Local and Global Resistor. *Langmuir* 32: 915–921.
11. Issadore D, Westervelt RM (2013) Point-of-care diagnostics on a chip. *Biological and Medical Physics, Biomedical Engineering Series*, Springer.
12. Gervais L (2011) Capillary microfluidic chips for point-of-care testing: from research tools to decentralized medical diagnostics. [PhD Thesis] *Ecole Polytechnique de Lausanne*.

13. Berthier J, Brakke KA, Furlani EP, et al. (2015) Whole blood spontaneous capillary flow in narrow V-groove microchannels. *Sens Actuators B.* 206: 258–267.
14. Merrill EW (1969) Rheology of blood. *Physiol Rev* 49: 863–888.
15. Brooks DE, Goodwin JW, Seaman GVF (1970) Interactions among erythrocytes under shear. *J Appl Physiol* 28: 172–177.
16. Apostolidis AJ, Beris AN (2014) Modeling of the blood rheology in steady-state shear flows. *J Rheol* 58: 607–633.
17. Chien S (1970) Shear dependence of effective cell volume as a determinant of blood viscosity. *Science* 168: 977–979.
18. McEwen MP, Reynolds KJ (2012) Light Transmission Patterns in Occluded Tissue: Does Rouleaux Formation Play a Role? *Proceedings of the World Congress on Engineering* Vol I WCE 2012, London, U.K.
19. Fedosov DA, Pan W, Caswell B, et al. (2011) Predicting human blood viscosity in silico. *PNAS* 108: 11772–11777.
20. Vand V (1948) Viscosity of solutions and suspensions. *J Phys Colloid Chem* 52: 300–314.
21. Fahraeus R, Lindqvist T (1931) The viscosity of blood in narrow capillary tubes. *Am J Physiol* 96: 562–568.
22. Herschel WH, Bulkley R (1926) Konsistenz-messungen von Gummi-Benzollösungen. *Kolloid-Z.* 39: 291–300.
23. Steffe JF (1996) Rheological Methods in Food Process Engineering 2nd. *Freeman Press*.
24. Bingham EC (1922) Fluidity and Plasticity. *McGraw-Hill, New York*.
25. Morhell N, Pastoriza H (2016) Power law fluid viscometry through capillary filling in a closed microchannel. *Sens Actuators B* 227: 24–28.
26. Cito S, Ahn YC, Pallares J, et al. (2012) Visualization and measurement of capillary-driven blood flow using spectral domain optical coherence tomography. *Microfluid Nanofluid* 13: 227–237.
27. Rabinowitsch B (1929) Uber die Viskosität und Elastizität von Solen. *A Physic Chemie* A 145: 1–26.
28. Mooney M (1931) Explicit formulas for slip and fluidity. *J Rheol* 2: 210–221.
29. Rosina J, Kvasnák E, Suta D, et al. (2007) Temperature dependence of blood surface tension. *Physiol Res* 56: S93–98.
30. Cherry EM, Eaton JK (2013) Shear thinning effects on blood flow in straight and curved tubes. *Phys Fluids* 25: 073104-1-19.
31. Quéré D (1997) Inertial capillarity. *Europhys Lett* 39: 533–538.
32. Bracke M, Voeght FD, Joos P (1989) The kinetics of wetting: the dynamic contact angle, in *Trends in Colloid and Interface Science III*, P. Bothorel and E. J. Dufourc, Eds. Steinkopff, 142–149.
33. Berthier J, Gosselin D, Delapierre G (2015) Spontaneous Capillary Flow: Should a Dynamic Contact Angle be Taken into Account ? *Sens Transducers J* 191: 40–45.
34. Berthier J, Brakke K, Berthier E (2014) A general condition for spontaneous capillary flow in uniform cross-section microchannels. *Microfluid Nanofluid* 16: 779–785.

Appendix

Appendix A: Dynamics of the capillary flow of a Herschel-Bulkley fluid

In the general case of incompressible fluids the Navier-Stokes equation writes:

$$\rho \frac{D\vec{v}}{Dt} = -\vec{\nabla}P + \vec{\nabla}\cdot\bar{\bar{\tau}} + \rho\,\vec{f} \tag{A.1}$$

where ρ is the fluid density, $\vec{v}$ is the flow velocity vector, t is the time, P is the pressure, $\bar{\bar{\tau}}$ is the deviatoric stress tensor and $\vec{f}$ the body forces.

Assuming a uniform cross-section channel and a laminar flow—which is the general case in microfluidics, where the Reynolds number is small—there is a unique velocity component—denoted *v*—directed along the *x*-axis.

Additionally, assuming that there are no external forces—such as gravity, because of the small dimensions and horizontality of the system—, relation (A1) simplifies to

$$\rho \frac{Dv}{Dt} = -\frac{\partial P}{\partial x} + \nabla\cdot\overrightarrow{\tau_x} \tag{A2}$$

Moreover remarking that the continuity equation implies that $\frac{\partial v}{\partial x} = 0$, relation (A.2) can be written as

$$\rho \frac{\partial v}{\partial t} = -\frac{\partial P}{\partial x} + \nabla\cdot\overrightarrow{\tau_x} \tag{A.3}$$

Upon integration of (A.3) on the fluid volume in the channel between the channel inlet and the front of the flow and using the Gauss-Ostrogradski theorem, one obtains

$$\rho\, x(t) S\, \frac{\partial \bar{v}}{\partial t} = -A\,\Delta P + \oiint_{S_w} \tau_w \overrightarrow{dS} \tag{A.4}$$

where A is the cross-section of the duct, $\bar{v}$ is the average flow velocity in a cross-section, $x(t)$ is the penetration distance, S_w is the wetted surface of the duct, τ_w is the wall friction, and ΔP the drop pressure over the flow.

An average wall friction can be introduced, defined by

$$\overline{\tau_w} = \frac{1}{p_w}\oint_\Gamma \tau_w dl \tag{A.5}$$

where p_w is the wetted perimeter in a cross-section and Γ the wetted contour. Substitution of (A.5) in (A.4) yields

$$\frac{\partial \bar{v}}{\partial t} = -\frac{\Delta P}{\rho}\frac{1}{x(t)} + \frac{p_w}{\rho\, A}\,\overline{\tau_w} \tag{A.6}$$

According to (3), the wall friction of a Herschel-Bulkley fluid reads as

$$\tau_w = \left(\frac{\tau_0}{|\dot{\gamma}_w|} + K|\dot{\gamma}_w|^{n-1}\right)\dot{\gamma}_w, \tag{A.7}$$

where $\dot{\gamma}_w$ is the shear rate at the wall defined by $\dot{\gamma}_w = \partial V(r)/\partial\vec{n}|_w < 0$. V(r) is the velocity field over the cross section. To be consistent with the Gauss-Ostrogradski theorem used for (A.4) $\vec{n}$ is the outward unit-vector normal to the wall. As represented in figure 2, one can define a friction length λ by

$$\bar{v} = -\lambda \frac{\partial V(r)}{\partial \vec{n}}\Big|_w \tag{A.8}$$

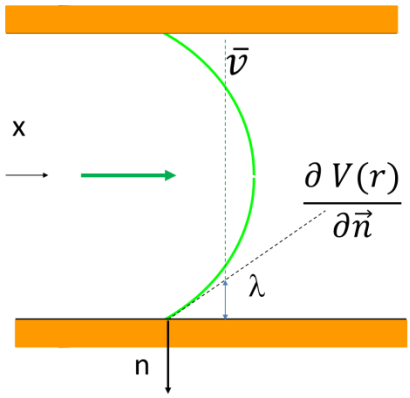

Figure A.1. Definition of the friction factor from the velocity profile.

Substituting relation (A.7) in (A.5) and using the parameter λ yields

$$\overline{\tau_w} = -\tau_0 - \frac{K}{p_w}\oint_\Gamma \left(\frac{\bar{v}}{\lambda}\right)^n dl \tag{A.9}$$

If we define the average generalized friction length $\overline{\lambda^n}$ [6] by

$$\frac{1}{\overline{\lambda^n}} = \frac{1}{p_w}\oint_\Gamma \frac{1}{\lambda^n}\, dl, \tag{A.10}$$

relation (A.9) can be cast under the form

$$\overline{\tau_w} = -\tau_0 - \frac{K}{\overline{\lambda^n}}\,\bar{v}^n\,. \tag{A.11}$$

And finally the differential equation (A.6) writes

$$\frac{d^2x}{dt^2} + \frac{p_w}{\rho\, A}\frac{K}{\overline{\lambda^n}}\left(\frac{\partial x}{\partial t}\right)^n + \frac{\Delta P}{\rho\, x(t)} = -\frac{p_w}{\rho\, A}\tau_0 \tag{A.12}$$

Equation (A.12) is a second order differential equation where the only remaining unknown parameter is the friction length $\overline{\lambda^n}$. The pressure drop ΔP is given by the capillary pressure (Laplace pressure) with the convention of an inlet pressure null in reference to the atmosphere.

$$\Delta P \;=\; P_{cap} - P_{in} \;=\; P_{cap} \;=\; -\frac{F_{cap}}{A} \;=\; -\frac{\gamma p_w \cos\theta^*}{A} \tag{A.13}$$

where θ^* is the generalized Cassie angle which takes into account the wetting on the different walls and air in the case of composite or open channels [34]. Using (A.13), (A.12) can be cast under the following form:

$$\frac{d^2x}{dt^2} + \frac{p_w}{\rho\, A}\frac{K}{\overline{\lambda^n}}\left(\frac{\partial x}{\partial t}\right)^n - \frac{\gamma p_w \cos\theta^*}{\rho\, A\, x(t)} \;=\; -\frac{p_w}{\rho\, A}\tau_0 \tag{A.14}$$

The following appendix focuses on the calculation of the average friction length $\overline{\lambda^n}$ in the particular case of a cylindrical duct made of a single material.

Appendix B: Calculation of the average friction length for a cylindrical duct.

The expression (A.8) can be written

$$\frac{1}{\lambda} \;=\; -\frac{1}{\bar{v}}\frac{\partial V(r)}{\partial \vec{n}}\bigg|_w \tag{B.1}$$

which shows that the friction length can be determined from the velocity field.

Thus we need to calculate the velocity profile v(r) and the mean velocity $\bar{v}$ for a flow within a cylindrical duct

Determination of the velocity profile

Let us first calculate the velocity profile from the general Navier-Stokes equation

$$\rho\,\frac{D\vec{v}}{Dt} \;=\; \rho\left(\frac{\partial \vec{v}}{\partial t} + \vec{v}\cdot\vec{\nabla}\vec{v}\right) \;=\; -\vec{\nabla}P + \vec{\nabla}\cdot\,\bar{\bar{\tau}} + \rho\vec{f} \tag{B.2}$$

A velocity profile at a given location is determined by the local cross section of the channel, the rheological behavior of the fluid (both through the stress tensor), the local pressure gradient and the body forces that applied at this location. Hence to determine the velocity profile over a given cross section one can consider a steady-state flow through this same cross section where the fluid rheology, the pressure gradient and the body forces become parameters. In our case we can thus consider a steady-state flow through a cylindrical duct. Thus the left hand side of (B.2) is zero. Besides in the case of a horizontal channel, the body forces are null, and equation (B.2) simplifies to

$$G \;=\; \frac{\partial P}{\partial x} \;=\; \frac{\partial \tau}{\partial r} + \frac{1}{r}\tau \tag{B.3}$$

with

$$\tau \;=\; \left(K|\dot{\gamma}|^{n-1} + \frac{\tau_0}{|\dot{\gamma}|}\right)\dot{\gamma} \;=\; -\tau_0 - K\left(-\frac{\partial v}{\partial r}\right)^n \tag{B.4}$$

Note that since we are dealing with a uniform channel, the pressure decreases linearly along the channel. Hence G is a constant with respect to x.

Substituting (B.4) in (B.3) gives

$$G = -\frac{\tau_0}{r} - K\frac{1}{r}\frac{\partial}{\partial r}\left(r\left(-\frac{\partial v}{\partial r}\right)^n\right) \tag{B.5}$$

Hence

$$\frac{rG}{K} + \frac{\tau_0}{K} = -\frac{\partial}{\partial r}\left(r\left(-\frac{\partial v}{\partial r}\right)^n\right) \tag{B.6}$$

Integrating (B.6) in respect to r— which is possible since G does not depend on r —yields

$$\frac{r^2 G}{2K} + \frac{\tau_0}{K} r = -r\left(-\frac{\partial v}{\partial r}\right)^n \tag{B.7}$$

or

$$-\frac{\partial v}{\partial r} = \sqrt[n]{-\frac{rG}{2K} - \frac{\tau_0}{K}} = \left(\frac{-G}{2K}\right)^{\frac{1}{n}} (r - R_0)^{\frac{1}{n}} \tag{B.8}$$

where $R_0 = -\frac{2\tau_0}{G}$. Note that r = R_0 is the radius where the velocity profile flattens. Physically in the region where $r < R_0$, the shear is too small and the liquid has a constant velocity, i.e. it behaves as a solid.

Denoting $c = \frac{R_0}{R}$, a second integration for r ≥ R_0 (with the no slip condition at the wall, i.e. v(R) = 0) yields the following velocity distribution

$$v(r) = \left(\frac{-G}{2K}\right)^{\frac{1}{n}} R^{\frac{n+1}{n}} \frac{n}{n+1}\left[(1-c)^{\frac{n+1}{n}} - \left(\frac{r}{R} - c\right)^{\frac{n+1}{n}}\right] \tag{B.9}$$

Within this region, the velocity has a profile as a power law of exponent *n/(n+1)*. Note that if *n* = 1 and $\tau_0 = 0$, one regains the Newtonian expression.

In the central region, the constant velocity, independent of r, is given by

$$v(R_0) = \left(\frac{-G}{2K}\right)^{\frac{1}{n}} R^{\frac{n+1}{n}} \frac{n}{n+1}(1-c)^{\frac{n+1}{n}} \tag{B.10}$$

Remark that in the case where $\tau_0 = 0$ (and $n \neq 1$), the fluid is called a "power-law" fluid, i.e. $\tau = \mu\,\dot{\gamma}^n$, and the velocity profile in a cross-section has been derived by Rabinowitsch and Mooney [23,27,28]. In such a case, $R_0 = 0$ (no yield stress), and relation (B.9) simplifies to

$$v = \left(\frac{(\delta P)}{2KL}\right)^{\frac{1}{n}} \frac{n}{n+1}\left[R^{\frac{n+1}{n}} - r^{\frac{n+1}{n}}\right] \tag{B.11}$$

where $\frac{\delta P}{L}$ is the pressure gradient. Relation (B.11) is exactly the profile derived by Rabinowitsch and Mooney.

Determination of the mean velocity

As stated in the beginning of this appendix we also need the mean velocity to calculate the friction length (B.1). Thus let us now determinate the mean velocity $\bar{v}$ of the flow in a cross-section. Integration of the velocity profile over a cross section yields

$$\bar{v} = \frac{1}{\pi R^2}\iint v_x d\sigma = \frac{1}{\pi R^2}\int_0^{2\pi}\int_0^R v\, r dr d\theta = \frac{2}{R^2}\left(\int_0^{R_0} v\, r dr + \int_{R_0}^R v\, r dr\right)$$

$$= \frac{2}{R^2}\left(\frac{v(R_0)}{2}\int_0^{R_0} dr^2 + \int_{R_0}^R v\, r dr\right) \quad \text{(B.12)}$$

Note that we have introduced the radius R_0 because of the constant velocity—noted $v(R_0)$—inside the disc $r < R_0$.

Substituting (B.9) and (B.10) in (B.12) leads to

$$\bar{v} = \frac{2}{R^2}\left[\left(\frac{-G}{2K}\right)^{\frac{1}{n}}\frac{n}{n+1}R^{\frac{n+1}{n}}(1-c)^{\frac{n+1}{n}}\frac{R_0^2}{2} + \left(\frac{-G}{2K}\right)^{\frac{1}{n}}\frac{n}{n+1}R^{\frac{n+1}{n}}\int_{R_0}^R\left(r\,(1-c)^{\frac{n+1}{n}} - r\left(\frac{r}{R}-c\right)^{\frac{n+1}{n}}\right)dr\right] \quad \text{(B.13)}$$

Integration of (B.13) yields

$$\bar{v} = \frac{2}{R^2}\left(\frac{-G}{2K}\right)^{\frac{1}{n}}\frac{n}{n+1}R^{\frac{n+1}{n}}\left[(1-c)^{\frac{n+1}{n}}\frac{R_0^2}{2} + (1-c)^{\frac{n+1}{n}}\frac{(R^2-R_0^2)}{2} - \int_{R_0}^R r\left(\frac{r}{R}-c\right)^{\frac{n+1}{n}}dr\right] \quad \text{(B.14)}$$

Some algebra is required to transform the integral at the right hand side of (B.14). Let us use the auxiliary variable $u = \frac{r}{R} - c$. Then

$$\int_{R_0}^R\left(\frac{r}{R}-c\right)^{\frac{n+1}{n}} r\,dr = R\int_0^{1-c} u^{\frac{n+1}{n}}(u+c)\,du = R\left[\int_0^{1-c} u^{\frac{2n+1}{n}}du + c\int_0^{1-c} u^{\frac{n+1}{n}}du\right] \quad \text{(B.15)}$$

Finally,

$$\int_{R_0}^R\left(\frac{r}{R}-c\right)^{\frac{n+1}{n}} r\,dr = R^2\,(1-c)^{\frac{2n+1}{n}}\left[\frac{n}{3n+1}(1-c) + \frac{n}{2n+1}\,c\right] \quad \text{(B.16)}$$

The expression of the average velocity is then

$$\bar{v} = \frac{2}{R^2}\left(\frac{-G}{2K}\right)^{\frac{1}{n}}\frac{n}{n+1}R^{\frac{n+1}{n}}\left\{(1-c)^{\frac{n+1}{n}}\frac{R_0^2}{2} + (1-c)^{\frac{n+1}{n}}\frac{(R^2-R_0^2)}{2} - R^2\,(1-c)^{\frac{2n+1}{n}}\left[\frac{n}{3n+1}(1-c) + \frac{n}{2n+1}\,c\right]\right\} \quad \text{(B.17)}$$

or

$$\bar{v} = \left(\frac{-G}{2K}\right)^{\frac{1}{n}} \frac{n}{n+1} R^{\frac{n+1}{n}} (1-c)^{\frac{n+1}{n}} \left\{1 - 2(1-c)\left[\frac{n}{3n+1}(1-c) + \frac{n}{2n+1}\, c\right]\right\} \quad \text{(B.18)}$$

Determination of the average friction length

For simplicity of calculation let us write the velocity profile according to the average velocity.

Upon substitution of (B.18) in (B.9) and (B.10), one finds the following expressions for the velocity profile

$$v = \frac{\bar{v}}{\alpha}\left[(1-c)^{\frac{n+1}{n}} - \left(\frac{r}{R} - c\right)^{\frac{n+1}{n}}\right] \text{ for } r > R_0 \quad \text{(B.19)}$$

and

$$v = \frac{\bar{v}}{\alpha}(1-c)^{\frac{n+1}{n}} \text{ for } r < R_0 \quad \text{(B.20)}$$

where $= (1-c)^{\frac{n+1}{n}}\left\{1 - 2(1-c)\left(\frac{n}{3n+1}(1-c) + c\frac{n}{2n+1}\right)\right\}$, $c = \frac{R_0}{R}$ and $R_0 = -\frac{2\tau_0}{G}$.

It can easily be verified that when $n = 1$ and $\tau_0 = 0$, $\alpha = 1/2$, then $= 2\bar{v}\left(1 - \frac{r^2}{R^2}\right)$, which is the well-know profile for Newtonian fluids.

Let us now calculate the friction length by substituting Eq (B.19) into Eq (B.1):

$$\frac{1}{\lambda} = \left(\frac{n+1}{n}\frac{1}{R\,\alpha}\right)(1-c)^{1/n} \quad \text{(B.21)}$$

Given the cylindrical symmetry of our channel, the average friction length writes:

$$\frac{1}{\overline{\lambda^n}} = \frac{1}{p_w}\oint_\Gamma \frac{1}{\lambda^n}\, dl = \frac{1}{\lambda^n} = \left(\frac{n+1}{n}\frac{1}{R\,\alpha}\right)^n (1-c) \quad \text{(B.22)}$$

where p_w is the length of the wetted perimeter and Γ the perimeter of the channel.

Note that Expression (B.22) is consistent with the Newtonian case ($n = 1$ and $\tau_0 = 0$) for which $R_0 = 0$, $c = 0$, $\alpha = 1/2$ and $\bar{\lambda} = \frac{R}{4}$ [6].